A simple methods for downscaling passive microwave based soil moisture

O. Merlin, G. Chehbouni, J.P. Walker, R. Panciera, Y.H. Kerr

▶ To cite this version:

HAL Id: ird-00390430
http://hal.ird.fr/ird-00390430

Submitted on 2 Jun 2009

Passive microwave soil moisture downscaling using evaporative fraction

Olivier Merlin[1]

Abdelghani Chehbouni[2]

Jeffrey P. Walker[1]

Rocco Panciera[1]

Yann Kerr[2]

[1] Department of Civil and Environmental Engineering, University of Melbourne, Australia

[2] Centre d'Etudes Spatiales de la Biosphère, France

Abstract—This paper develops two different approaches for downscaling (disaggregation) passive microwave derived soil moisture from coarse resolution L-band observations. Ground and airborne data collected over Walnut Gulch experimental watershed during the Monsoon '90 experiment were used to test these approaches. These data consisted of eight micro-meteorological stations (METFLUX) and six flights of the L-band Push Broom Microwave Radiometer (PBMR). For each PBMR flight, the 180m resolution L-band pixels covering the eight METFLUX sites were first aggregated to generate a 500m "coarse-scale" passive microwave pixel. The coarse-scale derived soil moisture is then downscaled to 180m resolution using two different surface soil moisture indices (SMIs): i) the evaporative fraction (EF), which is the ratio of the evapotranspiration to the total energy available at the surface; and ii) the actual evaporative fraction (AEF), defined as the ratio of the actual to potential evapotranspiration. It is well known that both SMIs depend on surface soil moisture. However, they are also influenced by other factors such as vegetation cover, soil type, and atmospheric conditions. In order to decouple the influence of soil moisture from the other factors, a land surface model was used in conjunction with a projection technique to account for the heterogeneity of vegetation cover, soil type, and atmospheric conditions. The projection increased the coefficient correlation between SMIs and surface soil moisture from 0.66 to 0.79 for EF and from 0.71 to 0.81 for AEF. When comparing the downscaled soil moisture obtained with EF and AEF, it is apparent that AEF is more directly linked to surface soil moisture, especially for high soil moisture values. Those results illustrate the potential use of high-resolution satellite-based estimates of instantaneous evapotranspiration acquired on clear-sky days for downscaling coarse-resolution passive microwave soil moisture.

Index Terms—Downscaling, passive microwave, surface soil moisture, evapotranspiration, evaporative fraction.

I. INTRODUCTION

Soil moisture is one state variable that controls several earth surface related processes, including hydrology, meteorology, climate modelling, and agricultural management. It controls the portioning of rainfall into infiltration and runoff, and thus influences strongly the response of stream discharge to rainfall events, and playing a key role in the prediction of erosion and sediment loads in watershed streams and ponds [1]. Soil moisture also controls the partitioning of available energy at the surface into sensible and latent heat fluxes, which triggers development of the atmospheric boundary layer. Soil moisture is also a key variable for sustainable management of irrigation water, which consumes about 85% of total available surface water in arid and semi-arid regions [2]. In moisture limited regions, soil moisture content has also been used as an indicator of the spatial distribution of precipitation and general plant health [3].

The spatial and temporal dynamics of soil moisture is very complex since it depends on several factors. Beside the weather conditions, it also depends on a variety of surface features such as land cover/land use, topography and geology. One feasible way of monitoring this variability is through a dense network of continuous observation of soil moisture. This can be done for a confined experimental area during short periods but the establishment of a continuous in situ soil moisture monitoring program worldwide is not practical and economically feasible. Consequently, the only possibility for deriving the spatially distributed soil moisture data required for the applications mentioned above, is through use of satellite observations. Satellite-based soil moisture can be obtained from passive microwave or active microwave sensors through to the large contrast between the dielectric properties of liquid water (≈ 80) and those of dry soil (≈ 4), and the resulting variability on dielectric properties of soil-water mixtures as they go from dry to wet ($\approx 4 - 30$).

Active microwave sensors such as the European satellites ERS-1/2 C-band Synthetic Aperture

Radar (SAR), ENVISAT C-band Advanced SAR, and the Canadian C-band RADARSAT-1/2 can provide resolutions from 10 to 100 m over a swath width of 50–500 km, which meet the spatial requirement for most basin-scale hydrological applications [4]. However, despite the multitude of models developed during the last decade to infer soil moisture from the backscatter coefficient, the issue of decoupling the effect of surface roughness and vegetation biomass from that of soil moisture is still unanswered. To date, no operational algorithm exists to invert soil moisture from SAR data –at least– with the existing space borne sensors [5].

Passive microwave sensors represent an interesting alternative for monitoring soil moisture [6]. The ability of passive microwave space-borne sensors such as the Scanning Multichannel Microwave Radiometer (SMMR), the Special Sensor Microwave Imager (SSMI) and the Advanced Microwave Scanning Radiometer (AMSR-E) to provide a daily global coverage makes them very useful for several earth science disciplines. Airborne sensors which are operating at low frequencies (L-Band), such as the Push-Broom Microwave Radiometer (PBMR) and the Electronically Scanned Thinned Array Radiometer (ESTAR) have been found very effective for inferring surface soil moisture [7]. In this context, the Soil Moisture and Ocean Salinity (SMOS) mission [8] operating at L-band is scheduled for launch by European Space Agency (ESA) in mid 2008. This instrument is based on an innovative two-dimensional aperture synthesis concept, which will bring new and significant capabilities in terms of multi-angular viewing configurations and will allow for simultaneously retrieving soil moisture and vegetation biomass [9,10] with a revisit time ranging from 1 to 3 days and a mean ground resolution (pixel size) of about 40km. This instrument will provide a valuable global data set of soil moisture content to be implemented in general circulation and climate models. However, the use of coarse spatial resolution of instrument such as SMOS in the field of hydrology is not straightforward [11]. Indeed, the scale at which most hydrological processes are better observed and modelled is

less than 1km [12]. It is thus of crucial importance to develop simple and robust procedures to disaggregate passive microwave-based soil moisture from its nominal scale to that needed for hydrologic application and/or watershed management.

In this context, several disaggregation approaches with different degrees of complexity have been developed during the last decade. Without going into a comprehensive review of all existing methods which is beyond the scope of this paper, they can be categorised into three groups:

i) methods based on the use of topography and soil depth information [13];

ii) methods based on the combination of passive microwave data with high spatial resolution active microwave data [14] or optical data such as surface temperature and vegetation index [15]; and

iii) methods based on the combination of coarse resolution passive microwave data, with fine-scale optical data and a surface process model [16,12].

This paper follows from that of [16], but with two fundamental differences. The two differences are: i) there is no need to have dual angle observations of surface temperature; and ii) a simple energy balance model can be used in place of a complex surface process model. Two different energy balance approaches are developed and tested for downscaling (disaggregating) the coarse resolution passive microwave derived soil moisture that can be retrieved from L-band radiometry. These two approaches are based on two different soil moisture indices (SMIs): i) the evaporative fraction (EF), which is the ratio of the evapotranspiration to the total energy available at the surface; and ii) the actual evaporative fraction (AEF), which is computed as the ratio of the actual to potential evapotranspiration. The hypothesis is that these indices, which can be computed at fine spatial resolution, can provide information on the fine scale distribution of surface soil moisture. The projection technique developed in [16] is then implemented with a surface energy balance model to decouple the effects of external factors (i.e. land cover, soil

properties, meteorological forcing) on the relationships between SMIs and surface soil moisture. Ground and airborne data collected over the Walnut Gulch experimental watershed during the Monsoon'90 experiment were used to test the performance of these two approaches. These data consisted of eight micro-meteorological stations (METFLUX) and six flights of the L-band PBMR. For each PBMR flight, the 180m resolution L-band pixels covering the eight METFLUX sites were first aggregated to generate a 500m resolution "coarse-scale" passive microwave pixel. The coarse resolution derived soil moisture is then downscaled using the two approaches outlined above, and evaluated against the ground-based data. The applicability of such downscaling methods to SMOS scale is finally discussed in a separate section.

II. MONSOON'90 DATA

The Monsoon '90 experiment was conducted during the summer of 1990 over the USDA-ARS Walnut Gulch Experimental Watershed (WGEW) in southeastern Arizona, USA [17,18]. The purpose of the experiment was to remotely sense moisture fluxes in a semiarid climate during a dry-down. A network of eight meteorological surface energy flux (METFLUX) stations covering the main study area (about 150 km^2) were situated in grass-dominated and shrub-dominated ecosystems and in the transition zones containing both vegetation types. The data collected at each METFLUX site from Julian day (Jd) 204 to Jd 222 consist of 20 minute estimates of: 0-5cm soil moisture, meteorological conditions at screen height including air temperature, relative humidity, wind speed and solar radiation, surface fluxes composed of net radiation, soil heat flux measured at -5 cm, sensible heat flux and latent heat flux.

As part of the Monsoon'90 campaign, the NASA PBMR was flown on six flights of the C-130 aircraft during a 10-day period in July and August of 1990 [19]. The objective was to map the surface brightness temperature at a wavelength of 21-cm (L band) and to infer surface soil moisture from these data. The 4 beams of PBMR point at ± 8° and ± 24° incidence angle with a

3dB beam width of about 30% of the altitude. For Monsoon '90 the PBMR flights were at an altitude of 600 m, which yielded an IFOV of 180m. Available PBMR data of the Monsoon '90 experiment are nadir H-polarized brightness temperatures. To create the images of the brightness temperature at nadir, the outer beams were corrected for incidence angle effects during each PBMR flight by multiplying them by the ratio of the average of the inner beam to the outer beam on each side [19].

In this study, a time series of six 500m resolution microwave pixels was generated by aggregating the eight closest 180m resolution PBMR pixels covering each of the eight METFLUX stations on each day of PBMR observations. The low resolution soil moisture is retrieved by using the linear regression of PBMR brightness temperature versus ground-based 0-5cm soil moisture derived by [19]. These coarse resolution soil moisture values are subsequently downscaled, using ground measurements of evapotranspiration. A discussion about the operational application of such methods to SMOS and optical sensors is provided.

III. METHOD

The surface soil moisture retrieved from generated coarse-scale microwave pixels is downscaled by using two fine-scale SMIs at the eight METFLUX sites: i) the evaporative fraction (EF) and ii) the actual evaporative fraction (AEF). The downscaling approaches are based on a linear relationship between surface soil moisture and the SMI. To decouple the effect of other factors on this relationship, the projection technique of [16] is used in conjunction with a surface energy balance model and surface properties at high resolution. The diagram of Figure 1 illustrates the different steps and parameters involved in the downscaling procedure.

The general idea behind the approach is to assume a linear relationship between a SMI and surface soil moisture, and scale this relationship at high resolution with the observed low resolution soil moisture, and the slope of the correlation between the SMI and surface soil

moisture. The slope (noted f_1) of the correlation between the SMI and surface soil moisture is therefore assumed to be invariant across scales i.e. f_1 is constant in space within the microwave pixel. In the paper, parameter f_1 is also assumed to be constant in time due to the constancy of EF/AEF during most daytime. This allows calibrating it during a training period, independently from the application data set.

A.   General approach

Assuming a linear relationship between surface soil moisture and the SMI, the downscaled soil moisture values W_H (subscript $_H$ for high resolution = 180m) can be expressed as:

$$W_H = W_{L,obs} + f_{1,L}\left(SMI_{H,obs} - <SMI_{H,obs}>\right) \tag{1}$$

with $W_{L,obs}$ (subscript $_L$ for low resolution = 500m and subscript $_{obs}$ for observed) being the coarse-scale soil moisture retrieved from the aggregated PBMR data, $SMI_{H,obs}$ the high resolution SMI measured at the eight METFLUX sites, $<SMI_{H,obs}>$ the SMI averaged at the low resolution and $f_{1,L}$ the slope of the correlation between surface soil moisture and the SMI. In [16], the SMI was the soil temperature inverted from dual angle radiative surface temperature and the slope f_1 was retrieved from SMOS observation by using the multi-angular, bi-polarized information of surface soil emission. As this information may be difficult to extract due to vegetation effects on SMOS observation, this papers tests other SMIs for which the f_1 parameter does not vary much in time and/or can be estimated indirectly from a different source of data. This is the rationale for choosing EF and AEF as SMIs. Both ratios are in general nearly constant during the daytime [20,21,22,23,24]. Moreover, they are more directly related to surface moisture condition [25] and less dependent on incoming radiation than evapotranspiration or surface temperature [26]. In the paper, parameter f_1 is therefore assumed to be constant in time. As it is also constant in space within the microwave pixel (hypothesis of

linearity of the correlation between SMI and surface soil moisture), the slope f_1 is assumed to be a constant. In the paper, it is calibrated using ground-based data during a training period.

B. Soil moisture indices

In the paper, EF and AEF are both calculated from the surface fluxes and meteorological data monitored at the eight METFLUX sites.

The observed EF is calculated as:

$$EF_{obs} = \frac{LE_{obs}}{Rn_{obs} - G_{obs}} \tag{2}$$

with LE_{obs}, Rn_{obs} and G_{obs} being the latent heat flux, the net radiation and the ground flux measured by the METFLUX stations. The observed AEF is calculated as:

$$AEF_{obs} = \frac{LE_{obs}}{LEp_{obs}} \tag{3}$$

with LEp_{obs} being the potential evapotranspiration computed with the Penman-Monteith formula:

$$LEp_{obs} = \frac{\Delta(Rn_{obs} - G_{obs}) + \rho C_p \left(\dfrac{e_s - e_{a,obs}}{r_a} \right)}{\Delta + \gamma \left(1 + \dfrac{r_{min}}{r_{a,obs}} \right)} \tag{4}$$

with $e_s - e_{a,obs}$ representing the vapor pressure deficit of the air, ρ being the mean air density at constant pressure, Cp the specific heat of the air, Δ the slope of the saturation vapor pressure temperature relationship, γ the psychrometric constant, $r_{a,obs}$ the aerodynamic resistance and r_{min} the minimum surface resistance (fixed to 20 for the eight METFLUX sites). The canopy height used to calculate the aerodynamic resistance is from [27].

As an illustration of the dependence of EF to surface soil moisture, Figure 2 shows the time series of surface soil moisture and evaporative fraction measured at the METFLUX stations.

Both the maximum and the minimum values measured at the eight METFLUX stations are plotted to illustrate the range of spatial variability observed within the coarse-scale microwave pixel. The difference between the maximum and minimum surface soil moisture varies from approximately 10 to 20 % vol. from Jd 212 to Jd 221. It is apparent that dynamics of EF plotted between 10am and 2pm is link to the dynamics of surface soil moisture observed in the period Jd 212 and Jd 221. The difference between the maximum and minimum values of EF varies between 0.2 and 0.5. Note that the values of EF greater than 1 are due to the presence of clouds, which make the energy available suddenly decrease while the surface is still evaporating.

The results of a synthetic study are presented in Figure 3. The surface energy balance model of [28] is used to simulate the variation of both ratios EF ann AEF in response to surface soil moisture ranging from 0 to 35% vol. and for different LAI values from 0.5 to 4. Atmospheric forcing is fixed (air temperature Ta = 20 °C; incoming radiation Rg = 900 Wm^{-2}; relative humidity qa = 50%; wind speed u = 3 ms^{-1}) and surface parameters are set as in [28]. The correlation between SMI and surface soil moisture appears to be non-linear above 20% vol., above which SMI tends to saturate. The use of EF and AEF as soil moisture index is therefore limited to soil moisture values below this threshold. The synthetic study also shows that the sensitivity of the SMI to surface soil moisture decreases with increasing LAI values.

C. Projection

The general idea behind the projection is to improve the correlation between the SMI and surface soil moisture at high resolution before applying the downscaling procedure of equation (1). The methodology used in the paper is the projection technique developed in [16]. It consists of using a land surface model to simulate the impact at high resolution of surface parameters such as vegetation cover, soil type and atmospheric conditions on the correlation between the SMI and surface soil moisture. In this paper, a simple surface energy balance model is used to

simulate EF/AEF at high-resolution given: i) surface parameters available at high resolution and, ii) the same set of surface parameters estimated at low resolution. The projected EF/AEF noted $\overline{SMI_{H,obs}}$ is written as the observed SMI subtracted by the difference of the two simulated SMIs:

$$\overline{SMI_{H,obs}} = SMI_{H,obs} - \left[SMI_{H,sim}\left(W_H, p_H\right) - SMI_{H,sim}\left(W_H, <p>_H\right)\right] \tag{5}$$

with $SMI_{H,sim}\left(W_H, p_H\right)$ (and subscript $_{sim}$ for simulated) being the SMI simulated using the surface parameters available at high resolution and $SMI_{H,sim}\left(W_H, <p>_H\right)$ the SMI simulated using the surface parameters averaged at the microwave resolution. The projected SMI is therefore a combination of the observed SMI and the SMI simulated by the surface energy model using fine- and integrated-scale surface parameters. Note that the projection does not require all the surface parameters involved in the surface energy budget (input of the model) to be available at high-resolution. If one parameter is available at high-resolution (vegetation cover for instance), the projection can be applied with respect to this parameter only.

By replacing the observed SMI by the projected SMI, the expression of the downscaled soil moisture of equation (1) is modified as follows:

$$W_H = W_{L,obs} + f_{1,L}\left(\overline{SMI_{H,obs}} - <\overline{SMI_{H,obs}}>\right) \tag{6}$$

Note that the application of equation (5) requires iterating on soil moisture values, as W_H is not known at the beginning of the procedure. In fact, the algorithm runs a loop on integer k with:

$$W_{H,k} = W_{L,obs}$$

(7)

for $k = 0$ (initialization) and:

$$W_{H,k} = W_{L,obs} + f_{1,L}\left(\overline{SMI(W_{H,k-1})} - <\overline{SMI(W_{H,k-1})}>\right)$$

(8)

for $k > 0$. Convergence of W_H is typically reached after two or three iterations on k. Note that W_H is the only parameter to vary in equation (8). In this paper, parameter f_1 is assumed to be constant in time and space (within the microwave pixel).

D. Land surface energy balance model

The energy balance model used for the application to the Monsoon '90 data is the N95 model developed by [28], revised by [29] and further improved by [30]. Briefly, it is a dual-source model treating the energy balance of the soil/substrate and vegetation using surface skin temperature observations at the zenith view angle [28] and remotely sensed images of near-surface soil moisture [29] for estimating the soil energy balance over the watershed of the Monsoon '90 experiment. In this study, the model revised by [29] is preferred because the heterogeneity of the 0-5 cm soil moisture is accounted for in the estimation of surface fluxes. The model formulation explicitly computes the soil evaporation as a function of the resistance of the top soil layer to water vapor transfer. The resistance of surface soil layer r_{ss} is parameterized with near-surface soil moisture [31]:

$$r_{ss} = \exp(A - BW/W_{sat})$$ (9)

with A and B being two calibration parameters and W_{sat} the soil moisture at saturation (35% vol. for the Walnuch Gulch site). Total net radiation Rn is partitioned into Rns and Rnc as in [28]:

$$\begin{cases} Rns = Rn \exp(-\kappa LAI) \\ Rnc = Rn[1 - \exp(-\kappa LAI)] \end{cases}$$ (10)

with κ is estimated to be 0.45 for high solar zenith angles.

The simulated SMI involved in equation (5) can be expressed as:

$$EF_{sim}(W, p) = \frac{LE_{sim}(W, p)}{Rn_{sim}(W, p) - G_{sim}(W, p)}$$ (11)

and:

$$AEF_{sim}(W,p) = \frac{LE_{sim}(W,p)}{LE_{sim}(W_{sat},p)}$$ (12)

with $LE_{sim}(W,p)$, $Rn_{sim}(W,p)$, $G_{sim}(W,p)$ and $LE_{sim}(W_{sat},p)$ being respectively the latent

heat flux, net radiation flux, ground heat flux, and potential latent heat flux simulated with the

N95 model. The N95 model is calibrated against EF observations during a training period

between Jd 206 and 211. The measured and simulated EF is averaged between 10am and 2pm

and the root mean square difference between the average of the measured and simulated EF is

minimized by varying the parameters A, B and LAI. Results of the site-specific calibration are

presented in Table I. The space varying surface parameters are composed of A, B, LAI, canopy

height, air temperature Ta, relative humidity qa, solar radiation Rg and wind speed u. The other

input parameters in p are fixed to uniform values as in [30].

IV. APPLICATION

Application of the downscaling approaches presented here include successively i) the

projection of EF and AEF, ii) the estimation of the slope f_1 and iii) downscaling the coarse-

resolution soil moisture retrieved from the six generated microwave pixels. The approach is

demonstrated using Monsoon'90 data and the downscaled results compared with ground-based

measurements.

The projection technique is applied to the data set between Jd 212 and Jd 221. The projected

EF and projected AEF are calculated using equation (6), averaged between 10am and 2pm and

compared to the 10am-2pm average of the measured EF and AEF from METFLUX stations.

Results are presented in Figure 4, where it is apparent that the correlation between SMI and W is

improved by the projection in both cases; the correlation coefficient is increased from 0.66 to

0.79 and from 0.71 to 0.81 for EF and AEF respectively. The projection is therefore a useful tool

to decouple the effect of other variables on the correlation between SMI and W, given that a surface energy model can be properly calibrated over heterogeneous areas, notably for different vegetation covers and soil properties.

The parameter f_1 in equation (5) is then calibrated by minimizing the root mean square difference between the soil moisture simulated with equation (5) and observations from Jd 206 to 211. The mean and standard deviation of f_1 is evaluated to 56 and 10, and 47 and 7 for EF and AEF respectively (f_1 is in % vol.). In our analysis, parameter f_1 is assumed to be a constant in time. The same mean value obtained between Jd 206 and 211 is therefore used in the application during PBMR flights. Note that the time period for the calibration of f_1 (Jd 206 to Jd 211) is different from the time period of the application (Jd 212 to 221). This allows testing of the assumption of that f_1 can be held constant, using an independent data set.

The soil moisture retrieved at coarse resolution from the six generated microwave pixels is then disaggregated with equation (5) using the projected SMIs and the value of the slope f_1 estimated previously. Downscaled soil moisture is plotted against observations in Figure 5 for both the EF and AEF approaches. Table II reports the mean root mean square error (RMSE) between the downscaled and measured soil moisture values for each of the six days of data. When using all parameters at high-resolution (meteorological data, soil and vegetation parameters), the average of the RMSE is about 2% (vol. per vol.) and 3% for AEF and EF respectively. On Jd 214 however, the disaggregation error is greater than 5% vol. in both cases. The poor correlation with ground observations on Jd 214 can be explained by (i) the great variations of f_1 with the presence of clouds (see time series of EF in Fig. 2) and (ii) the saturation of SMI for soil moisture values above 20% vol (see synthetic study in Fig. 3).

The comparison of downscaling results with EF and AEF shows that the AEF-based approach is more accurate in most cases. In Table II, the error on downscaled values is in general lower

(except on Jd 216) with the use of AEF. As the N95 model was calibrated against EF observations, and not against AEF observations, results with the EF approach were expected to be superior. While the projection technique improves the correlation between EF and W, as compared to AEF and W, the correlation between the measured AEF and surface soil moisture is simply higher. The stronger link between AEF and surface soil moisture can be explained by several factors.

First, AEF is intrinsically more directly linked to surface moisture status than EF, as AEF is defined relatively to a "wet-surface", whereas EF is defined relative to a surface at the "thermal equilibrium". In the case of bare soil in particular, various analyses have shown that AEF can be expressed as a function of solely near-surface soil moisture alone [32,33]. For vegetated surfaces, AEF is also dependent on vegetation characteristics and water potential in the root zone. However, one can argue that the normalization of AEF at saturation (AEF=1) makes this SMI more applicable to different vegetation covers in this range of soil moisture. Figure 2 illustrates how AEF scales with surface soil moisture, which is less dependent on LAI for high soil moisture values than EF.

The second explanation for a stronger link with AEF and soil moisture is that the diurnal variability of EF may limit the validity of the " f_1 constant" hypothesis in this case. The diurnal behaviour of EF depends on both surface conditions and atmospheric loading. Notably atmospheric demand for evapotranspiration is governed by solar radiation, relative humidity and, to a lesser extent, air temperature and wind speed; while surface control is exerted by soil moisture and vegetation condition. This issue has been heavily investigated from both experimental and theoretical perspectives [22,23,34]. Most of these studies have reported a typical concave-up shape for EF which can induce errors when assuming a daytime constant EF equal to the noon value, since the latter is always lower than the daily average [24]. The

assumption of the self conservation of EF during day time hour is only valid under relatively dry surface and clear sky conditions [21,34].

To check the stability of both SMIs with the Monsoon'90 data, the relative variability of EF and AEF is estimated by successively calculating the standard deviation of measurements at the eight METFLUX sites between 10am and 2pm, averaging the eight standard deviations, and normalizing the diurnal variability with the sensitivity of SMIs to surface soil moisture. The sensitivity of AE and AEF to surface soil moisture is evaluated as the difference between the SMIs calculated at 20% vol. (maximum value) and 0 (minimum value) using the linear regression of the correlations EF-W and AEF-W respectively. Table III lists the values of the relative diurnal variability (in %) of EF and AEF evaluated for each day between Jd 212 and Jd 222. The average diurnal cycle represents about 20% and 15% of the sensitivity to surface soil moisture for EF and AEF respectively. It is suggested that the superiority of the AEF-based approach is partly due to the relative stability of AEF for changing atmospheric conditions. In the case of EF, the assumption "f_1 constant" is less valid.

Finally, the comparison between the error on downscaled soil moisture in Table II and the diurnal variation of EF and AEF in Table III indicates that the performance of the dis-aggregation is well correlated with the stability of SMIs. For example, the disaggregation results are significantly improved on Jd 212, 217 and 221, for which the diurnal variability of AEF is approximately half that of EF. The temporal variability of atmospheric conditions is also presented in Table III for comparison with the diurnal variability of SMIs. The temporal variations of solar radiation, relative humidity, air temperature and wind speed are calculated as the spatial average at the eight METFLUX sites of the standard deviation between 10am and 2pm. It is apparent that variations in EF and AEF can be attributed to changes in solar radiation

and relative humidity; the impact of air temperature and wind speed being less visible with these data.

V. LIMITATIONS AND APPLICABILITY TO SMOS

Application to the Monsoon'90 data demonstrated the performance of the approach when using ground-based measurements over a limited range of surface conditions (8 locations distributed within a 150km^2 semi-arid area) and during a short period of time (20 days). This section aims to assess the applicability of the suggested method to SMOS like data at larger space-time scales. The assumptions underlying the development of equations (1) to (6) are listed and discussed. A sensitivity analysis of the algorithm is also conducted to evaluate the impact of uncertainties in ancillary data, high-resolution SMI observations and low-resolution surface soil moisture observations on the disaggregation results.

A. Assumptions

The methodology is based on five assumptions. Each assumption is followed by a discussion regarding its applicability to SMOS like data:

1) Cloud free conditions: evaporative fraction observations can be derived at large spatial scales using optical data [35,36,37], but optical data will be available for clear sky conditions only. Note that clear sky conditions are also needed, as shown in the application to Monsoon'90, to meet the "f_1 constant" hypothesis.

2) Soil moisture index observations are available at approximately the same time as passive microwave observations, so as the low resolution surface soil moisture does not vary much between the two types of observations. With daily optical data such as the MODerate resolution Imaging Spectroradiometer (MODIS), this requirement is generally

met: one can assume that the 40km soil moisture does not change significantly between 6am (SMOS overpass time) and 10am (MODIS overpass time).

3) The soil moisture index is assumed to be linearly correlated to surface soil moisture, which allows writing equations (1) and (6). The synthetic study of Fig. 3 showed that the relationship between EF/AEF and surface soil moisture is non-linear for high soil moisture values. The saturation of the SMI does not allow estimating high-resolution surface soil moisture above the saturation threshold (20% vol. in the case of the Walnut Gulch watershed). This represents a limitation of the downscaling method for applications where the studied process does not saturate above this soil moisture threshold.

4) Some parameters involved in the surface energy budget such as vegetation cover, soil properties, and meteorological forcing are assumed to be available at high resolution so as the projection technique of equation (5) can be used. It is however reminded that one parameter available at high resolution (e.g. LAI) is sufficient to apply the projection, as long as the other parameters can be estimated at low resolution.

5) The slope of the correlation f_1 between SMI and surface soil moisture is assumed to be relatively independent of meteorological forcing data. This allows :

   o using the projection technique with low-resolution meteorological data only; and

   o calibrating f_1 during a training period that is independent from the application data set. Note that the value of f_1 still varies with any changes in vegetation cover. The calibration of f_1 should therefore be undertaken for each microwave pixel, and as often as the surface conditions (seasons, land use) change within the microwave pixel.

B. Sensitivity analysis

To assess the impact of uncertainties in input data of the downscaling procedure, realistic measurement errors were added to high-resolution SMI and low-resolution surface soil moisture observations. Three cases are investigated:

i)   surface parameters such as vegetation characteristics (LAI, canopy height), soil properties (A,B), meteorological data (Rg,Ta,ua,qa) are available at low-resolution only (not at high-resolution as in the previous section);

ii)   a bias ranging from -5 to +5% vol. on the low-resolution soil moisture observation;

iii)   10% and 20% error on SMI observations with LAI ranging from 0 to 4.

For each of the three cases, the impact on the downscaled soil moisture is evaluated and discussed.

1) Surface parameters available at low-resolution only

To evaluate the impact of resolution of ancillary data, the downscaling procedure is run with the same data set as in the previous section, but with the surface parameters -composed of LAI, canopy height, soil resistance parameters, meteorological forcing data- averaged at the scale of the microwave pixel. Table II lists the mean RMSE on the downscaled soil moisture obtained for each type of ancillary information separately. Results are to be compared to the case where all surface parameters are available at high-resolution. It is apparent that the spatial resolution of soil resistance parameters and canopy height (ranging from 0.1 to 0.6m for Monsoon'90) has no significant impact on the disaggregation results. However, the impact of the resolution of LAI is more significant: the mean RMSE increased from 2.7% vol. to 3.7% vol. for EF and from 2.2% vol. to 2.8% vol. for AEF. The impact of resolution of meteorological data is very low for both EF and AEF. Surprisingly, downscaling results are slightly better in general with low-resolution than with high-resolution atmospheric forcing. It is suggested that the projection is not able to

correct efficiently the impact of meteorological conditions to the correlation between SMI and surface soil moisture, as this impact is rather small with EF and AEF.

As a summary, the critical ancillary data to be used at high resolution seem to be the LAI and soil parameters A and B. The resolution of meteorological data does not seem to have a significant impact on the downscaling results. Note however, that the spatial extent of the data set used in this paper is rather small ($150km^2$) compared to the SMOS pixel size ($1600km^2$), which means that higher heterogeneities are expected at the SMOS scale, with probably higher impacts on the downscaled soil moisture.

2) Bias on the low-resolution surface soil moisture observation

To evaluate the impact of a given bias on the low-resolution surface soil moisture observation to the downscaled soil moisture, a bias of -5, -4, -3, -2, -1, +1, +2, +3, +4 and +5% vol. was successively added to the low-resolution soil moisture observation. The resulting bias on the downscaled soil moisture W_H is plotted as function of the input bias on W_L in Figure 6 for EF and AEF separately. It is shown that the mean output bias is practically equal to the input bias, which confirms the linear link between high and low resolution surface soil moisture of equation (1) and (6). Note that the slight divergence of the high-resolution bias with respect to the 1:1 line for negative biases is due to the negative values of surface soil moisture that were forced to 0 in the simulations.

3) Uncertainty in remotely sensed evaporative fraction

Space-based estimates of evaporative fraction are probably more uncertain than the ground-based estimates acquired during a field experiment such as Monsoon'90. The objective is to simulate realistic uncertainties on space-based evaporative fraction observations and evaluate its impact on the disaggregation results. A synthetic study was undertaken to quantify the error on the downscaled soil moisture associated with an error of 10% and 20% on SMI estimates, and

with a LAI ranging from 0 to 4. Figure 6 illustrates the results obtained for EF and AEF separately. They indicate that an error of 5% vol. is achievable with 10% error on SMI. However, an error of 20% on SMI impacts significantly the downscaled soil moisture with an error estimated to 10% vol.

VI. CONCLUSIONS

Two simple approaches for downscaling (disaggregating) L-band coarse resolution passive microwave soil moisture are developed, and tested using ground and airborne data collected over the Walnut Gulch experimental watershed during the Monsoon'90 experiment. These data consisted of eight micro-meteorological stations and six flights of the L-band PBMR. For each PBMR flight, the L-band pixels covering the eight stations were first aggregated to generate a 500m coarse-scale passive microwave pixel. The soil moisture retrieved from the low resolution microwave observations was then downscaled to 180m, using two different SMIs to describe the sub-pixel variability of surface soil moisture: i) the ratio of the evapotranspiration to the available energy (EF); and ii) the ratio of the actual to potential evapotranspiration (AEF). It is well known that both SMIs depend on surface soil moisture. However, they are also influenced by other factors such as vegetation cover, soil type, and atmospheric conditions. In order to decouple the influence of soil moisture from the other factors, a surface energy balance surface model is used in conjunction with the projection technique developed in [16] to account for the heterogeneity of vegetation cover, soil type and atmospheric conditions.

The projection was able to increase the correlation coefficient between SMI and surface soil moisture from 0.66 to 0.79 and from 0.71 to 0.81 for EF and AEF respectively. The main hypothesis of the downscaling approaches is the constancy of the correlation between SMI and surface soil moisture (slope f_1) during day time. This assumption was considered valid in most cases given the overall accuracy on downscaled values of about 3% vol. for EF and 2% vol. for

AEF, except under cloudy conditions. The comparison of EF and AEF indicates that AEF is more directly linked to surface soil moisture, especially for high soil moisture values. The diurnal variability of EF due to temporal changes in incoming radiation and relative humidity seems to explain the superiority of the AEF-based approach.

The assumptions underlying the equations of the downscaling method were discussed in terms of their applicability to SMOS. When applied to the scale of about 40km (SMOS pixel size), the main limitations are: (i) optical derived SMI estimates limited to clear sky conditions, (ii) the saturation of SMI for high soil moisture values, which does not allow retrieving downscaled values above the saturation threshold (about 20% vol. with the Monsoon'90 data), and (iii) the availability of ancillary data such as meteorological data and soil/vegetation characteristics at high-resolution. Note however, that the availability of all the ancillary data at high resolution (notably meteorological data) is not a requirement to apply the projection.

A sensitivity analysis of the method was undertaken to assess the impact of uncertainties in input data to the downscaled soil moisture. An error of 10% on SMI observations has an effect of about 2 to 5% vol. on the downscaled soil moisture, depending on soil moisture and LAI values. A given bias on the low-resolution soil moisture observation impacts the downscaled soil moisture with the same bias.

Those results illustrate the potential use of high resolution satellite-based estimates of instantaneous evapotranspiration obtained on clear-sky days for downscaling coarse-resolution passive microwave soil moisture. Recent studies have investigated the use of 1km-resolution optical data such as NOAA/AVHRR and MODIS to develop operational schemes for monitoring EF at regional and global scales [35,36,37]. High-resolution microwave data collected during field experiments such as the National Airborne Field Experiment (NAFE) [38], will be essential

in testing downscaling methods before SMOS data become routinely available, and validating downscaled soil moisture products once SMOS is on orbit.

REFERENCES

[1] A. Western, R. Grayson, T. Green, "The Tarrawarra project: high resolution spatial measurement, modelling and analysis of soil moisture and hydrologic response," *Hydrol. Proc.*, vol. 13, pp. 633-652, 1999.

[2] A. Chehbouni, R. Escadafal, G. Boulet, B. Duchemin, V. Simmonaux, G. Dedieu, B. Mougenot, S. Khabba, H. Kharrou, O. Merlin, A. Chaponnière, J. Ezzahar, S. Erraki, J. Hoedjes, R. Hadria, H. Abourida, A. Cheggour, F. Raibi, L. Hanich, N. Guemouria, Ah Chehbouni, A. Olioso, F. Jacob and J. Sobrino, "The use of remotely sensed data for integrated hydrological modeling in arid and semi-arid regions: the SUDMED program," *Int. J. Remote Sens.*, submitted for publication.

[3] M. A. Perry, J. D. Niemann, "Analysis and estimation of soil moisture at the catchment scale using EOFs," *J. Hydrol.*, vol. 334, pp. 388-404, 2007.

[4] M. S. Moran, C. D. Peters-Lidard, J. M. Watts and S. McElroy, "Estimating soil moisture at the watershed scale with satellite-based radar and land surface models," *Can. J. Remote Sens.*, vol. 30, no. 5, pp. 805-826, 2004.

[5] W. Wagner, G. Bloschl, P. Pampaloni, J.-C. Calvet, B. Bizzarri, J.-P. Wigneron and Y. Kerr, "Operational readiness of microwave remote sensing of soil moisture for hydrologic applications," *Nordic Hydrol.*, vol. 38, no. 1, pp. 1-20.

[6] E. Njoku, E. Jackson, V. Lakshmi, T. Chan and S. Nghiem, "Soil moisture retrieval from AMSR-E," *IEEE Trans. Geosci. Remote Sens.*, vol. 41, pp. 215-229, 2003.

[7] T. J. Schmugge, "Applications of passive microwave observations of surface soil moisture," *J. Hydrol.*, vol. 212–213, pp. 188–197, 1998.

[8] Y. H. Kerr, P. Waldteufel, J.-P.Wigneron, J.-M. Martinuzzi, J. Font, and M. Berger, "Soil moisture retrieval from space: The Soil Moisture and Ocean Salinity (SMOS) mission," *IEEE Trans. Geosci. Remote Sens.*, vol. 39, no. 8, pp. 1729–1735, Aug. 2001.

[9] J.-P. Wigneron, J.-C. Calvet, T. Pellarin, A. Van De Griend, M. Berger, and P. Ferrazzoli, "Retrieving near surface soil moisture from microwave radiometric observations: current status and future plans," *Remote Sens. Environ.*, vol. 85, pp. 489–506, 2003.

[10] K. Saleh, J.-P. Wigneron, J.-P. Waldteufel, P. de Rosnay, J.-C. Calvet and Y. Kerr, "Estimates of surface soil moisture under grass covers using L-band radiometry", *Remote Sens. of Environ.*, submitted for publication.

[11] D. Entekhabi, G. R. Asrar, A. K. Betts, K. J. Beven, R. L. Bras, C. J. Duffy, T. Dunne, R. D. Koster, D. P. Lettenmaier, D. B. McLaughlin, W. J. Shuttleworth, M. T. van Genuchten, M.-Y. Wei and E. F. Wood, "An agenda for land surface hydrology research and a call for the Second International Hydrological Decade," *Bull. Am. Meteorol. Soc.*, vol. 80, no. 10, pp. 2043-2058, 1999.

[12] O. Merlin, A. Chehbouni, G. Boulet and Y. Kerr, "Assimilation of disaggregated microwave soil moisture into a hydrologic model using coarse-scale meteorological data," *J. Hydrometeor.*, vol. 7, no. 6, pp. 1308-1322, 2006.

[13] J. Pellenq, J. Kalma, G. Boulet, G.-M. Saulnier, S.Wooldridge, Y. Kerr, and A. Chehbouni, "A disaggregation scheme for soil moisture based on topography and soil depth," *J. Hydrol.*, vol. 276, pp. 112–127, May 2003.

[14] R. Bindlish and A. P. Barros, "Subpixel variability of remotely sensed soil moisture: An inter-comparison study of SAR and ESTAR," *IEEE Trans. Geosci. Remote Sens.*, vol. 40, no. 2, pp. 326–337, Feb. 2002.

[15] N. S. Chauhan, S. Miller, and P. Ardanuy, "Spaceborne soil moisture estimation at high resolution: A microwave-optical/IR synergistic approach," *Int. J. Remote Sens.*, vol. 24, no. 22, pp. 4599–4622, 2003.

[16] O. Merlin, A. Chehbouni, Y. Kerr, E. G. Njoku and D. Entekhabi, "A combined modeling and multi-spectral/multi-resolution remote sensing approach for disaggregation of surface soil moisture: Application to SMOS configuration," *IEEE Trans. Geosci. Remote Sens.*, vol. 43, pp. 2036-2050, 2005.

[17] W. P. Kustas, D. C. Goodrich, M. S. Moran, S. A. Amer, L. B. Bach, J. H. Blanford, A. Chehbouni, H. Claassen,W. E. Clements, P. C. Doraiswamy, P. Dubois, T. R. Clarke, C. S. T. Daughtry, D. I. Gellman, T. A. Grant, L. E. Hipps, A. R. Huete, K. S. Humes, T. J. Jackson, T. O. Keefer, W. D. Nichols, R. Parry, E. M. Perry, R. T. Pinker, P. J. Pinter, J. Qi, A. C. Riggs, T. J. Schmugge, A. M. Shutko, D. I. Stannard, E. Swiatek, J. D. van Leeuwen, J. van Zyl, A. Vidal, J. Washburne and M. A. Weltz, "An interdisciplinary field study of the energy and water fluxes in the atmosphere-biosphere system over semiarid rangelands: Description of some preliminary results," *Bull. Am. Meteorol. Soc.*, vol. 72, pp. 1683-1705, 1991.

[18]   W. P. Kustas and D. C. Goodrich, "Monsoon '90 multidisciplinary experiment," *Water Resources Res.*, vol. 30, pp. 1211-1225, 1994.

[19]   T. Schmugge, T. J. Jackson, W. P. Kustas, R. Roberts, R. Parry, D. C. Goodrich, S. A. Amer, and M. A. Weltz, "Push broom microwave radiometer observations of surface soil moisture in Monsoon '90," *Water Resour. Res.*, vol. 30, pp. 1321-1327, 1994.

[20]   W. J. Shutlleworth, R. J. Gurley, A. Y. Hsu and J. P. Ormsby, "FIFE: The variation in energy partition at surface flux sites," *IAHS Publ.*, vol. 186, pp. 67-74, 1989.

[21]   M. Sugita and W. Brutsaert, "Daily evaporation over a region from lower boundary-layer profiles measured with radiosondes," *Water Resour. Res.*, vol. 27, no. 5, pp. 742-752, 1991.

[22]   R. D. Crago, "Conservation and variability of the evaporative fraction during the daytime," *J. Hydrol.*, vol. 180, pp. 173-194, 1996.

[23]   R. Crago and W. Brutsaert, "Daytime evaporation and the self-preservation of the evaporative fraction and the Bowen ratio," *J. Hydrol.*, vol. 178, no. 1, pp. 241-255, April 1996.

[24]   P. Gentine, D. Entekhabi, A. Chehbouni, G. Boulet and B. Duchemin, "Analysis of diurnal evaporative fraction behavior," presented at the 83th AMS Annual Meeting, Atlanta, GA, 28-3 February 2006.

[25]   W. P. Kustas, T. J. Schmugge, K. S. Humes, T. J. Jackson, and R. Parry, "Relationships between evaporative fraction and remotely sensed vegetation index and microwave brightness temperature for semiarid rangelands," *J. Applied Meteorol.*, vol. 32, pp. 1781-1790, 1993.

[26]   K. Nishida, R. R. Nemani, S. W. Running and J. M. Glassy, "An operational remote sensing algorithm of land surface evaporation," *J. Geophys. Res.*, vol. 108, no. D9, p. 4270, doi:10.1029/2002JD002062, 2003.

[27] M. A. Weltz, J. C. Ritchie, H. D. Fox, "Comparison of laser and field measurements of vegetation height and canopy cover," *Water Resour. Res.*, vol. 30, no. 5, pp. 1311−1319, 1994.

[28] J. M. Norman, W. P. Kustas and K. S. Humes, "Source approach for estimating soil and vegetation energy uxes in observations of directional radiometric surface temperature," *Agr. For. Meteorol.*, vol. 77, pp. 263-293, 1995.

[29] W. P. Kustas, X. Zhan and T. J. Schmugge, "Combining optical and microwave remote sensing for mapping energy fluxes in a semiarid watershed," *Remote Sens. Environ.*, vol. 64, pp. 116-131, 1998.

[30] W. P. Kustas and J. M. Norman, "Evaluation of soil and vegetation heat flux predictions using a simple two-source model with radiometric temperatures for partial canopy cover", *Agr. For. Meteorol.*, vol. 94, pp. 13-29, 1999.

[31] P. J. Sellers, M. D. Heiser and F. G. Hall, "Relations between surface conductance and spectral vegetation indices at intermediate (100 m2 to 15 km2) length scales," *J. Geophys. Res.*, vol. 97, no. D17, pp. 19033-19059, 1992.

[32] K. E. Saxton, W. J. Rawls, J. S. Romberger, R. I. Papendick, "Estimating generalized soil-water characteristics from texture", *Soil Sc. Soc. Am. J.*, vol. 50, no. 4, pp. 1031-1036, 1986.

[33] T. S. Komatsu, "Toward a robust phenomenological expression of evaporative efficiency for unsaturated soil surfaces," *J. Applied Meteorol.*, vol. 42, no. 9, pp. 1330-1334, 2003.

[34] J.-P. Lhomme and E. Elguero, "Examination of evaporative fraction diurnal behaviour using a soil-vegetation model coupled with a mixed-layer model," *Hydrol. and Earth Syst. Sci.*, vol. 3, no. 2, pp. 259-270, 1999.

[35] L. Jiang and S. Islam, "Estimation of surface evaporation map over southern Great Plains using remote sensing data," *Water Resour. Res.*, vol. 37, no. 2, pp. 329-340, 2001.

[36] K. Nishida, R. R. Nemani, J. M. Glassy and S. W. Running, "Development of an evapotranspiration index from Aqua/MODIS for monitoring surface moisture status," *IEEE Trans. Geosci. Remote Sens.*, vol. 41, no. 2, pp. 493-501, 2003.

[37] K. Wang, Z. Li and M. Cribb, "Estimation of evaporative fraction from a combination of day and night land surface temperatures and NDVI: a new method to determine the Priestley-Taylor parameter," *Remote Sens. Environ.*, vol. 102, pp. 293-305, 2006.

[38] R. Panciera, J. Walker, J. Kalma, E. Kim, J. Hacker, O. Merlin and M. Berger, "The NAFE'05 data set: Towards SMOS calibration, downscaling and assimilation," *IEEE Trans. Geosci. Remote Sens.*, this issue.

TABLE I
Calibration parameters at the eight METFLUX sites.

Site	LAI	A	B
1	0.4	9	9
2	0.3	8	5
3	0.4	9	8
4	0.4	8	4
5	0.2	8	5
6	0.2	8	5
7	0.7	8	4
8	0.6	8	4

TABLE II

Mean root mean square error (RMSE) on the downscaled surface soil moisture for the six generated microwave pixels. Results obtained with EF and AEF, and with ancillary data available at high or low-resolution are successively presented.

Jd	RMSE (% vol.)									
	EF					AEF				
	High-resolution parameters	Low-resolution meteo data	Low-resolution soil parameters	Low-resolution LAI	Low-resolution canopy height	High-resolution parameters	Low-resolution meteo data	Low-resolution soil parameters	Low-resolution LAI	Low-resolution canopy height
212	**1.9**	1.8	2.6	2.5	2.0	**1.2**	1.3	1.9	1.7	1.2
214	**5.6**	5.0	6.3	6.0	6.0	**5.3**	5.3	5.6	5.6	6.2
216	**1.8**	1.9	2.4	3.0	1.7	**2.4**	2.1	2.6	3.1	2.5
217	**2.2**	2.2	1.9	3.8	2.0	**1.2**	1.4	1.4	2.0	1.3
220	**2.2**	1.9	1.8	3.2	2.6	**1.9**	1.5	2.2	2.8	2.0
221	**2.7**	2.3	2.5	2.8	3.0	**1.0**	1.2	1.1	1.9	1.2
Mean	**2.7**	2.5	2.9	3.6	2.9	**2.2**	2.1	2.4	2.8	2.4

TABLE III

Average at the eight METFLUX sites of the relative diurnal variability of EF and AEF, and standard deviation of solar radiation, relative humidity, air temperature and wind speed evaluated between 10am and 2pm for each day between Jd 212 and Jd 222. The six days of PBMR flight are underlined.

Jd	Relative variability (%)		σR_g	σq_a	σT_a	σu_a
	EF	AEF	(Wm^{-2})	$(^{\circ}C)$	$(^{\circ}C)$	(ms^{-1})
212	26	12	110	3.5	1.0	0.6
213	13	5	74	5.3	1.8	1.0
214	21	28	260	5.7	1.9	0.8
215	20	18	169	4.0	1.7	0.9
216	10	11	101	3.9	1.6	0.6
217	23	12	198	2.8	1.5	1.2
218	31	32	84	7.4	1.7	0.8
219	14	16	133	3.1	1.5	0.6
220	17	11	114	3.9	1.6	0.7
221	13	7	57	5.5	1.8	0.8
222	13	3	54	3.0	1.8	0.8

Figure captions

Figure 1. Schematic diagram of the downscaling procedure.

Figure 2. Time series of the (a) minimum and maximum surface soil moisture observed at the eight METFLUX sites and the (b) minimum and maximum evaporative fraction measured at the eight METFLUX sites between 10am and 2pm, from Jd 212 to Jd 221.

Figure 3. Sensitivity of the (a) simulated evaporative fraction (EF) and the (b) simulated actual evaporative fraction (AEF) to surface soil moisture for increasing LAI values.

Figure 4. Measured and projected soil moisture indices (SMIs) versus surface soil moisture observations between Jd 212 and Jd 221. The projected SMIs are also plotted versus measured SMIs for comparison.

Figure 5. Downscaled versus measured surface soil moisture for the six microwave pixels generated on Julian days 212, 214, 216, 217, 220 and 221. The results obtained with the (a) EF and (b) AEF are compared.

Figure 6. Estimated error on the downscaled soil moisture associated with a given uncertainty in SMI observations and a given bias on low-resolution soil moisture observations.
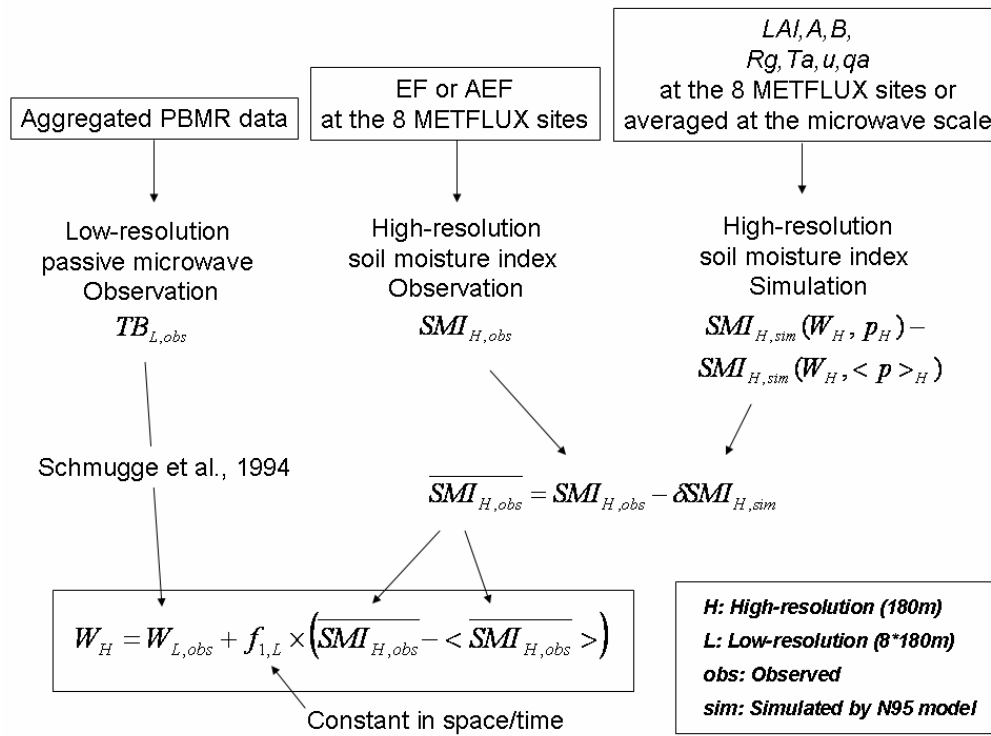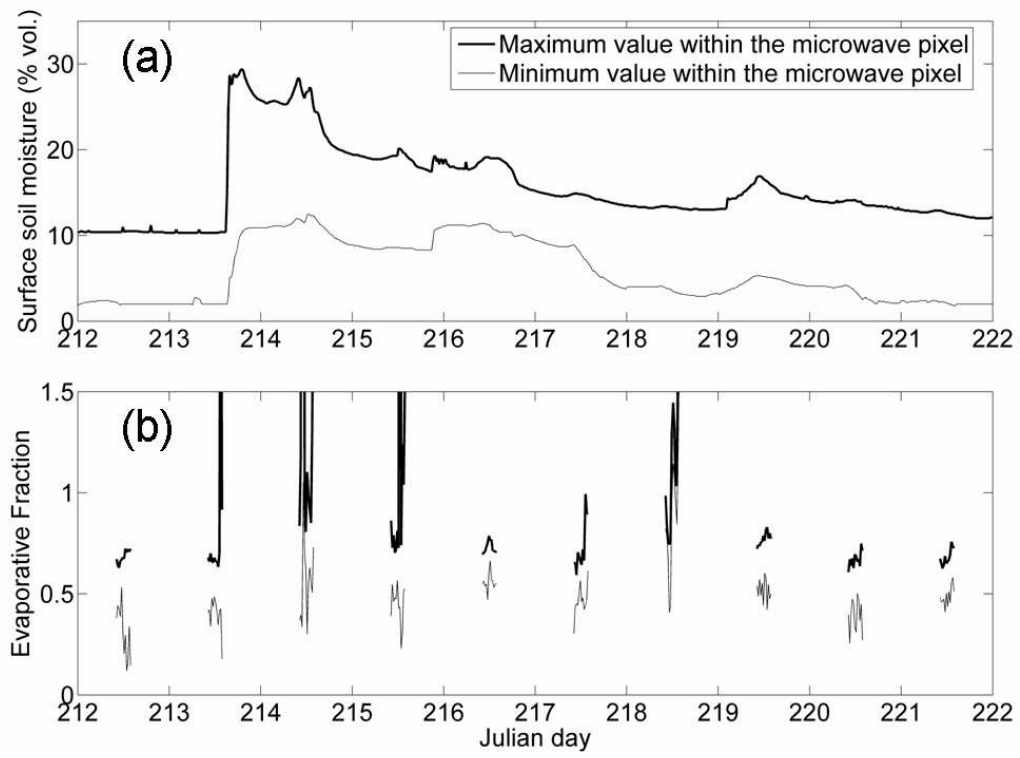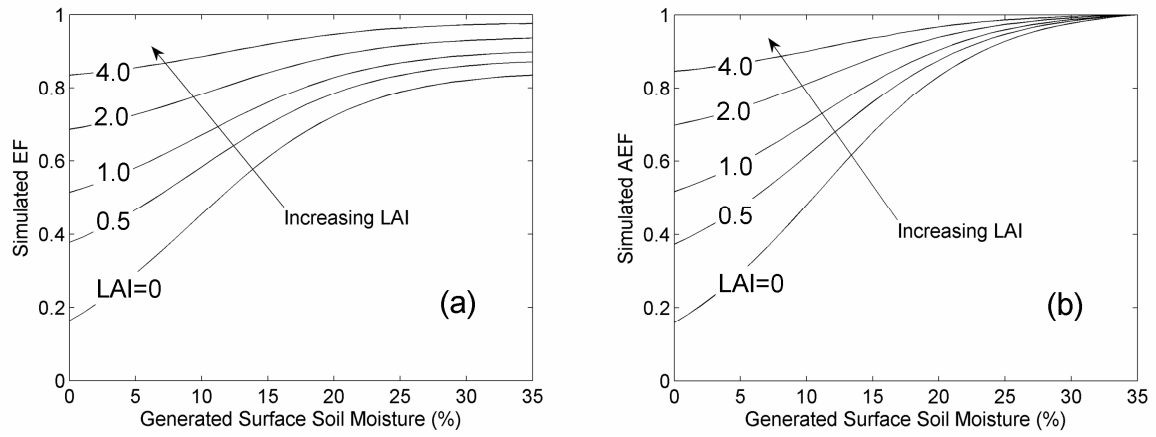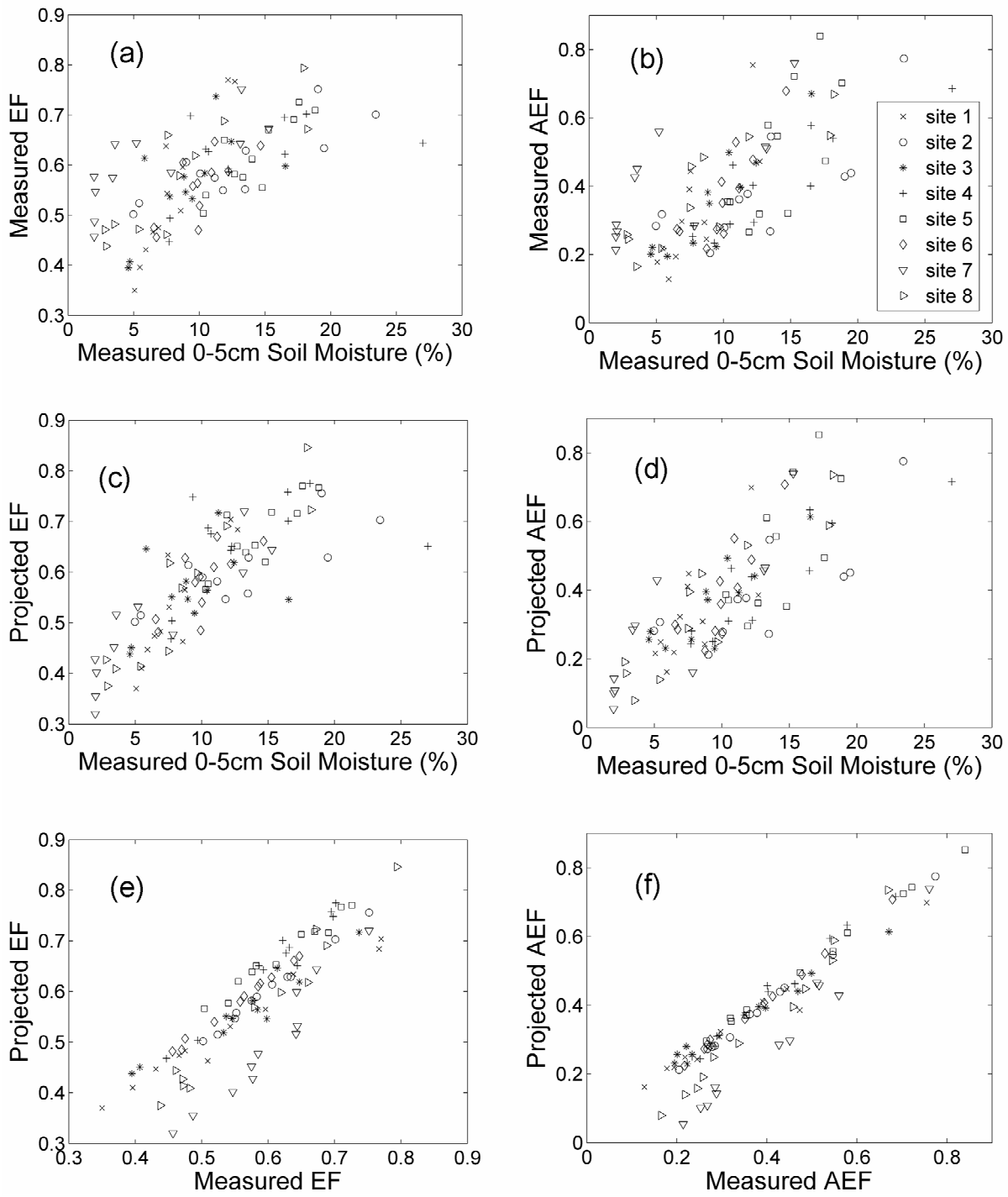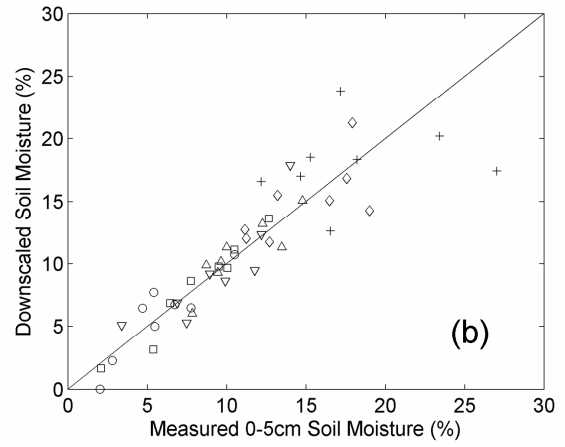
FIGURE 1

FIGURE 2

FIGURE 3

FIGURE 4

FIGURE 5

FIGURE 6